Oscillating Gradient Spin-Echo (OGSE) Diffusion Tensor Imaging of the Human Brain

Corey A. Baron and Christian Beaulieu*

Purpose: The dependence of diffusion tensor imaging (DTI) eigenvalues and fractional anisotropy (FA) on short diffusion times was investigated using oscillating gradient spin echo (OGSE) and pulsed gradient spin echo (PGSE) DTI in the human brain in vivo.

Theory and Methods: DTI was performed in seven healthy volunteers at 4.7 Tesla (T) with b = 300 s/mm^2 and diffusion times of 4.1 ms (OGSE 50 Hz), 7.4 ms (OGSE 25 Hz), 20 ms (PGSE), and 40 ms (PGSE). Eigenvalues and FA were compared in the corpus callosum body, splenium and genu, and the corticospinal, cingulum, inferior fronto-occipital, superior and inferior longitudinal fasciculi using tractography, and the thalamus and putamen using region-of-interest.

Results: Relative to 40 ms, the 4.1 ms diffusion time led to significant increases in DTI eigenvalues in seven white matter tracts (6% to 20% parallel, 13% to 40% perpendicular) and both deep gray matter regions (16% parallel, 18% to 26% perpendicular), and reductions of FA (−9% to −12%) in four tracts.

Conclusion: DTI eigenvalues and FA depend on diffusion time in both white and gray matter in the human brain. The ability to target different length scales by means of the diffusion time may improve sensitivity to changes in tissue microstructure associated with pathology. **Magn Reson Med 72:726–736, 2014.** © **2013 Wiley Periodicals, Inc.**

Key words: DTI; OGSE; diffusion time; human; eigenvalue; diffusion

INTRODUCTION

The apparent diffusion coefficient (ADC) measured using diffusion tensor imaging (DTI) depends on the time allowed for diffusing water molecules to probe the local environment; namely, the effective diffusion time (Δ_{eff}). If, during the diffusion time, most molecules do not travel far enough to interact with any obstacles, the measured ADC will be equivalent to the intrinsic diffusion coefficient (1,2). For increasing diffusion times, the molecules will interact with more barriers and the ADC will decrease, eventually reaching an asymptotic lower value; thus, measuring diffusion time dependence of ADC values may give insight into the microstructure (3).

DTI is typically performed using pulsed gradient spin-echo (PGSE) diffusion encoding (4), which has an inherently large Δ_{eff}, typically greater than 30 ms for in vivo human studies. The minimum diffusion time attainable while maintaining a desired level of diffusion sensitization (i.e., b-value) is limited by the maximum gradient strength. Early investigations using strong insert gradients demonstrated the dependence of ADC on Δ_{eff} in various excised nerves (5–8) and rodents (9). The minimum Δ_{eff} ranged from 1–4 ms and yielded increases of approximately a factor of 2 in perpendicular diffusion coefficients for short relative to long Δ_{eff} (5–8). While no changes in parallel diffusion coefficients were observed in one case (5), increases in parallel ADC by approximately a factor of 1.5 were observed in other studies (6,7). Lower diffusion anisotropy with decreasing Δ_{eff} was also reported in general (5–7). In contrast, there have been no findings of Δ_{eff}-dependence (with constant b-value) in human brain using PGSE or combinations of bi-polar pulsed gradients with Δ_{eff} ranging from 8 ms to 256 ms (10–12). The equivalent diffusion distances in water at body temperature for these diffusion times ranges from 7–39 μm and, given that axon diameters in the human corpus callosum range from 0.5–3 μm (13,14), most axons in these studies were likely in a restricted regime for all Δ_{eff}. Therefore, shorter diffusion times, as shown in the preclinical studies mentioned above, are presumably necessary to observe the onset of diffusion restriction in the human brain.

The oscillating gradient spin-echo (OGSE) method enables reduced Δ_{eff} by using a succession of short diffusion weighting periods (15–17). The use of bipolar gradient pulses to achieve small Δ_{eff} in some earlier studies was similar (5,9,11); however, OGSE theory additionally considers the frequency content of the diffusion gradients, which enables the design of optimal gradient waveforms. Moreover, OGSE waveforms enable the measurement of MRI signal with unique dependencies on intracellular properties (18), and may provide a means of quantitative measurements of cell characteristics, such as nuclear size and surface to volume ratios (19,20). A recent study in an in vivo rat model reported increases of mean ADC in cortical and subcortical gray matter as diffusion time decreased from 9.75 ms to 0.38 ms (21). Another study in an in vivo mouse brain with diffusion times ranging from 15 ms to 1.67 ms observed enhanced tissue contrast between different cell types in the hippocampus at the shortest diffusion times (22). The same study also showed increases in diffusion tensor eigenvalues (parallel and perpendicular) and decreases in fractional anisotropy (FA) in various white and gray matter regions with a reduction of Δ_{eff}. Similar OGSE DTI results in both white and gray matter have been observed in the in vivo

Department of Biomedical Engineering, Faculty of Medicine and Dentistry, University of Alberta, Edmonton, Alberta, Canada.

*Correspondence to: Christian Beaulieu, Ph.D., Department of Biomedical Engineering, Faculty of Medicine and Dentistry, Room 1098 Research Transition Facility, University of Alberta, Edmonton, Alberta, Canada T6G 2V2. E-mail: christian.beaulieu@ualberta.ca

Received 13 June 2013; revised 24 August 2013; accepted 15 September 2013

DOI 10.1002/mrm.24987

Published online 18 October 2013 in Wiley Online Library (wileyonlinelibrary.com).

rat brain with Δ_{eff} ranging from 7.5 ms to 1.88 ms (23). The additional sensitivity to intracellular structure provided by OGSE may provide insight into pathology. For example, the aforementioned study of the rat brain observed that the mean ADC decrease observed after a global ischemic event was approximately 50% lower for a Δ_{eff} of 0.5 ms compared with 9.75 ms, which suggests that half of the ischemic ADC decrease is from microstructure sensitive to diffusion times shorter than 0.5 ms (21). A recent study examining ADC characteristics in a rat glioma cell culture upon ischemia (Δ_{eff} ranging from 40 ms to 0.83 ms) concluded that at long diffusion times ischemia-induced ADC decreases in intracellular water result from changes in cell size and cellular volume fraction, while at short diffusion times ADC decreases are from changes in the intrinsic properties of the intracellular water (24). Additionally, it has been proposed that sensitivity to cell nuclear size may make OGSE useful in the monitoring of tumors (19,25,26).

The exploration of Δ_{eff}-dependence of diffusion in the human brain could enable greater insight into the mechanisms behind disease and their progression. First, though, an understanding of diffusion time dependence of DTI measurements is required in the healthy human brain. There has been one publication reporting Δ_{eff}-dependence of ADC measurements at constant b-value in humans, using OGSE gradients with a tetrahedral-encoding scheme and b = 200 s/mm^2 (27). The mean ADC in the corpus callosum showed a tendency to increase in four subjects with Δ_{eff} from 20 to 4 ms. The purpose of this work is to investigate the Δ_{eff} dependence of the full diffusion tensor in white and gray matter regions of healthy subjects by comparing OGSE and PGSE DTI with b = 300 s/mm^2 and Δ_{eff} ranging from 4–40 ms.

THEORY

The OGSE method uses the multiple application of short duration diffusion sensitizing periods (i.e., multiple bipolar pulses of gradients) to achieve a low Δ_{eff}, as shown in Figure 1a–d. Because the individual diffusion weighting periods are adjacent to each other, they cannot be considered independent. As such, the diffusion time for OGSE is better understood by recasting the diffusion tensor to a frequency-dependent form, D(f), where the signal attenuation, S/S_0, is described by (15,28):

$$\ln(S/S_0) = -\int F(f)D(f)F(f)df \qquad [1]$$

where F(f) characterizes the frequency content of the diffusion sensitizing gradients, G, and is given by

$$F(f) = -\int_0^{\infty}\left(\int_0^{t}\gamma G(\tau)d\tau\right)e^{i2\pi ft}dt \qquad [2]$$

where γ is the gyromagnetic ratio. F(f) can be intuitively understood as the Fourier transform of the wave number, k. It is clear from Eq. [1] and Eq. [2] that the signal attenuation is only sensitive to frequency components that are present in F(f). It has been shown that cosine gradients apodized with sinusoidal lobes at twice the target frequency produces a gradient modulation power spectra, $|F(f)|^2$, that is narrow around the desired

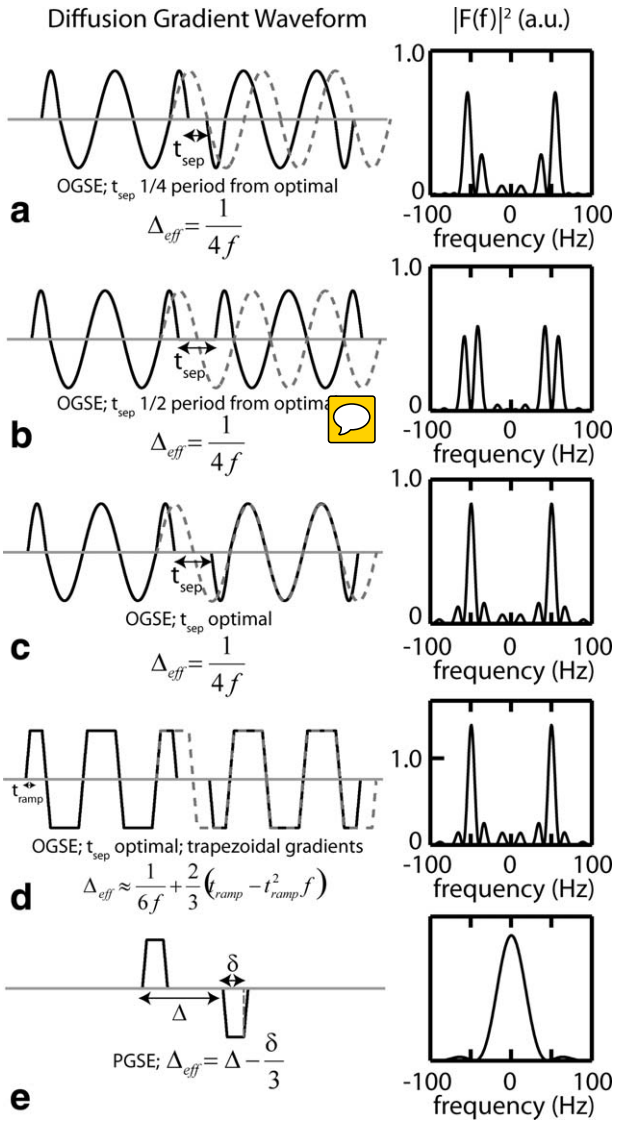

FIG. 1. Diffusion gradient waveforms and gradient modulation power spectra, $|F(f)|^2$, for OGSE (**a–d**) and PGSE (**e**). The polarity of the second gradient waveform has been reversed from what is actually played out to account for the 180° RF pulse that is between the gradient waveforms (RF pulses omitted from diagrams), and $|F(f)|^2$ is numerically calculated directly from the time-domain waveforms. The OGSE waveforms are cosine-modulated, with the start and end quarter-periods replaced with a twice-frequency sinusoid lobe. The separation between gradient waveforms, t_{sep}, is required to accommodate the 180° RF pulse. In (a–d), the dashed lines show that if t_{sep} is a value that allows a continuous single frequency oscillating gradient to be drawn between the two waveforms, narrower $|F(f)|^2$ are obtained. It is evident in (c,d) that trapezoidal gradients result in a negligible change in the shape of $|F(f)|^2$ relative to the sinusoidal gradients; however, it does increase the relative spectral amplitude enabling larger b-values. The duration of the shorter lobes in the trapezoidal case are increased by half the gradient ramp time, t_{ramp}, to ensure zero cumulative gradient area. The relationship for Δ_{eff} depends on the gradient shape, and is shown below each gradient waveform.

frequency (21,28). For such a gradient waveform the diffusion time is given by $\Delta_{eff} = 1/(4f)$.

Additionally, the separation and polarity between the two gradient waveforms before and after the 180° RF pulse affects the diffusion frequency spectra (27). Figure 1a–c shows that a separation, t_{sep}, which allows a continuous, unbroken sinusoid to be drawn across the two waveforms results in the most narrow spectral shape. Because sinusoids are not efficient for achieving large b-values, trapezoidal gradient waveforms are used in this work to enable an increase in b-value by 67% over the sinusoidal variant (27,29). There is almost no difference in the shape of F(f) for the trapezoidal case (Fig. 1c,d), because integrating the gradient before performing the Fourier transform in Eq. [2] results in a very similar spectra for the two waveform types; however, the amplitude of the trapezoidal $|F(f)|^2$ at the desired frequency is 69% larger than the sinusoidal version, reflecting it's increased b-value. As with the sinusoidal shape, for the trapezoidal gradient shape there is an optimal t_{sep} where a continuous oscillating trapezoidal gradient can be drawn across the waveforms (Fig. 1d). Using the same procedure as Gross and Kosfeld (15) and Parsons et al (28), the relationship between Δ_{eff} and f for the trapezoidal waveform is derived here to be

$$\Delta_{eff} = \frac{1}{6f} + \frac{2}{3}t_{ramp} - \frac{t_{ramp}^2}{6(1/4f - t_{ramp}/2)} + \frac{(2N+1)t_{ramp}^3}{120N(1/4f - t_{ramp}/2)} \approx \frac{1}{6f} + \frac{2}{3}(t_{ramp} - t_{ramp}^2 f) \quad [3]$$

where t_{ramp} is the gradient ramp time from zero gradient to the maximum gradient value and N is the total number of periods in both the gradient waveforms combined. Interestingly, the trapezoidal gradients are characterized by smaller diffusion times than the original cosine shape (for the same oscillation frequency) because of the larger b-values that are attained. The b-value is given by $b = 2N\gamma^2G^2(0.25/f - t_{ramp}/2)^2\Delta_{eff}$, where G is the maximum gradient amplitude. For PGSE, F(f) is broad and centered at a frequency of zero (Fig. 1e), and the diffusion time is given by $\Delta_{eff} = \Delta - \delta/3$ (Fig. 1e).

METHODS

Image Acquisition

Four DTI protocols were acquired per session in seven healthy human subjects (four male / three female; age 28 ±4 years) on a Varian Unity Inova 4.7 Tesla (T) MRI using Δ_{eff} = 4.1 ms (OGSE 50 Hz), 7.4 ms (OGSE 25 Hz), 20 ms (PGSE), and 40 ms (PGSE). The protocol parameters are summarized in Table 1. All protocols used b = 300 s/mm^2 with six diffusion encoding directions. Note that for low b-values, such as the case here, OGSE and PGSE gradient waveforms with the same Δ_{eff} have been shown to provide similar measurements of ADC (30). The six direction diffusion encoding scheme permits maximum gradient amplitude on two channels simultaneously that allows for b-values 2 times larger than from schemes with many directions (e.g., 30 directions). The

Table 1
DTI Protocols

Δ_{eff} (ms)	f (Hz)	Waveform type	δ (ms)[a]	Periods[b]	b (s/mm^2)	Scan time (min)
4.1	50	OGSE	4.4	2	300	10
7.4	25	OGSE	9.7	1	300	10
20	0	PGSE	5.7	–	300	10
40	0	PGSE	3.9	–	300	10

[a]For OGSE, the effective pulse width is given by 0.25/f – t_{ramp}/2.
[b]The number of periods on each side of the 180° RF pulse.

50 Hz OGSE protocol used two periods per gradient waveform with a maximum gradient of 57.5 mT/m per channel, while the 25 Hz OGSE protocol used 1 period per gradient waveform with a maximum gradient of 28.1 mT/m, thereby maintaining an equal total diffusion gradient time and b-value compared with the 50 Hz protocol. The number of periods are limited to prevent excessively long echo time (TE). For the 50 Hz scan, t_{sep} was 1/8 of a wavelength from the optimal value (the closest possible while maintaining the shortest possible TE), while t_{sep} was optimal for the 25 Hz scan. A conservative net slew rate of only 70 T/m/s was used to avoid peripheral nerve stimulation. Both PGSE protocols used a maximum gradient amplitude of 57.5 mT/m per channel, and used δ = 3.9 ms and Δ = 41.3 ms for the Δ_{eff} = 40 ms scan, and δ = 5.7 ms and Δ = 21.9 ms for the Δ_{eff} = 20 ms scan. Other single-shot EPI imaging parameters were as follows: repetition time (TR) = 12.5 s; TE = 110 ms; field of view = 24 cm; 2 mm × 2 mm acquired in-plane resolution (zero-filled to 1 mm × 1 mm resolution); 40 slices, thickness 2.5 mm; 6 averages; R = 2 GRAPPA (generalized autocalibrating partial parallel acquisition; scan time 10 min per protocol. Note that the TR (and scan time) was slightly lengthened to mitigate gradient heating that occurs due to the high duty cycle of the OGSE gradients.

A potential concern for this study was differing eddy currents for each diffusion gradient scheme; however, this was mitigated by using gradient precompensation (31,32). Any remaining eddy currents were evaluated by measuring them directly using a signal point source. The maximum gradient from any eddy current in any of the four protocols was less than 35 μT/m (0.1% of frequency encode gradient) at the beginning of the data readout, and exponentially decayed to less than 5 μT/m at TE (0.02% of frequency encode gradient). Thus, eddy current induced gradients were not expected to impact any findings from this study. Conversely, a transient B_0 eddy current (~1 ppm at beginning of data readout and 0.03 ppm at TE for OGSE 50 Hz; all other scans had a smaller B_0 eddy current) was found to degrade image quality if not accounted for. The phase imparted by the B_0 eddy current was found to be consistent with repeated acquisitions, and it was modeled by applying a least squares exponential fit to the phase accrual directly measured using a small 3 mm diameter probe sample. Then, the phase accrual was subtracted from the phase of the raw subject data before EPI image reconstruction. The effectiveness of the correction is shown in Figure 2.

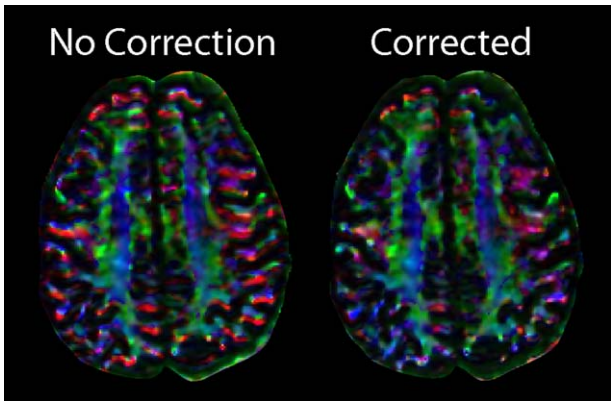

FIG. 2. FA color coded with principal eigenvalue direction with and without the phase correction for a transient B_0 eddy current, which causes nonuniform image shifts that vary with diffusion gradient direction. By applying a phase correction in k-space, incorrect directionality is ameliorated in the periphery. [Color figure can be viewed in the online issue, which is available at wileyonlinelibrary.com.]

Fiber Tracking and Statistical Analysis

ExploreDTI used an FA threshold of 0.2 and angle threshold of 30° for tractography of the body (bCC), splenium (sCC), and genu (gCC) of the corpus callosum, corticospinal tracts (CST), cingulum (CG), inferior fronto-occipital fasciculus (IFO), superior longitudinal fasciculus (SLF), and inferior longitudinal fasciculus (ILF) bilaterally. Examples of tractography and the regions used for diffusion parameter analysis are shown in Figure 3. Only central core regions were used for analysis to reduce errors that can occur from mis-registration of the four scans due to bulk patient motion and partial volume effects for the narrow tract extensions into the cortex (Fig. 3). The thalamus (TH) and putamen (PT) were delineated using manual region-of-interest (ROI) placement on multiple axial slices on the b = 0 s/mm^2 (b0) images. ROIs were placed on all slices that the TH or PT could be clearly identified; as such, the number of slices used varied with each subject. The data from the four scans were rigid-body motion corrected relative to each other using in-house auto-correlation based registration software. Voxels for analysis were chosen using the tract mask (or volumetric ROI for gray matter) obtained from the Δ_{eff} = 40 ms scan to yield parallel ($\lambda_{||}$) and perpendicular ($\lambda_{\perp}$) eigenvalues and fractional anisotropy (FA). A potential limitation was misalignment of the tract voxel mask across the four scans. Because eddy currents were effectively mitigated using gradient precompensation and correction methods, differences in eddy current distortions between the scans were not observed. Also, rigid body motion was corrected using registration and proper alignment of the data sets was confirmed before analysis for each subject. The scans and DTI analysis were performed on four different occasions for a 22°C, 14 cm diameter water phantom doped with $CuSO_4$ to evaluate diffusion parameter consistency over the four DTI protocols in a homogeneous, unrestricted environment. Statistical significance of overall Δ_{eff}-dependence was evaluated using a repeated measures analysis of variance (ANOVA), and changes with respect to the Δ_{eff} = 40 ms scans were evaluated using paired t-tests if the ANOVA reported a *P*-value less than 0.05.

The relatively small b-value of 300 s/mm^2 (b300) could potentially result in low quality data because the signal difference between the b0 and diffusion weighted images is smaller compared with typical b = 1000 s/mm^2 (b1000)

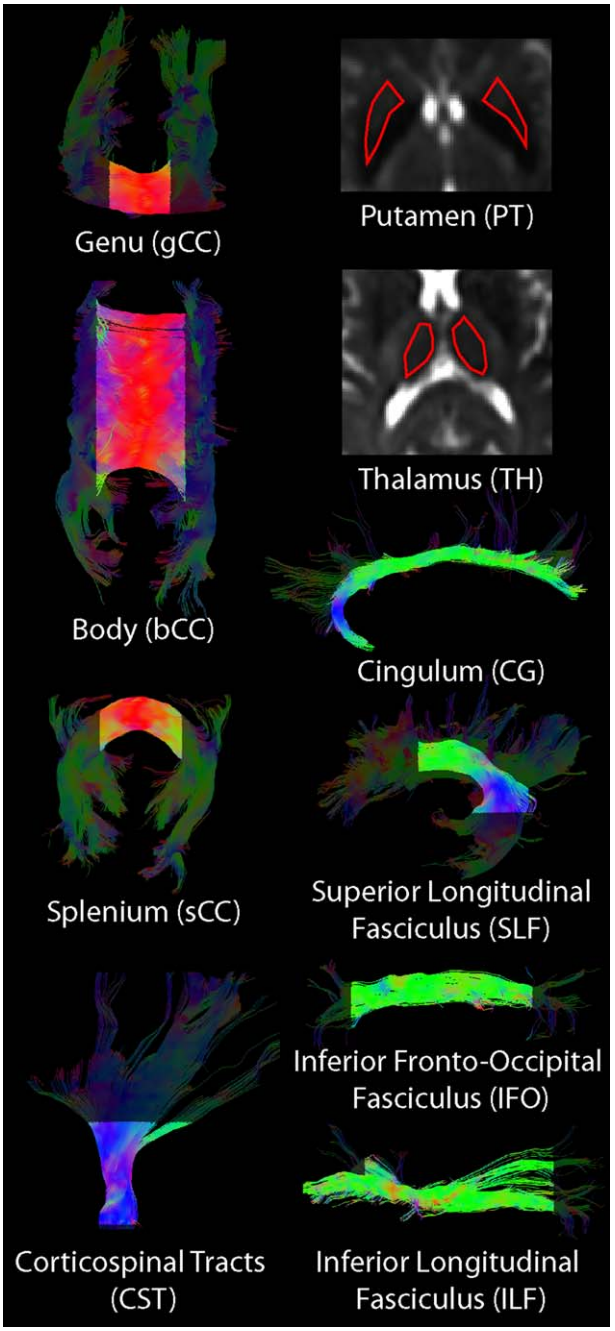

FIG. 3. Examples of tractography for eight white matter tracts using the Δ_{eff} = 40 ms scan, where tracts are color-coded with principal eigenvector direction, and ROI placement for the thalamus and putamen in one subject. The thin tract portions extended into the cortical areas (semitransparent portions of the shown tracts) were excluded from analysis to minimize partial volume effects. [Color figure can be viewed in the online issue, which is available at wileyonlinelibrary.com.]

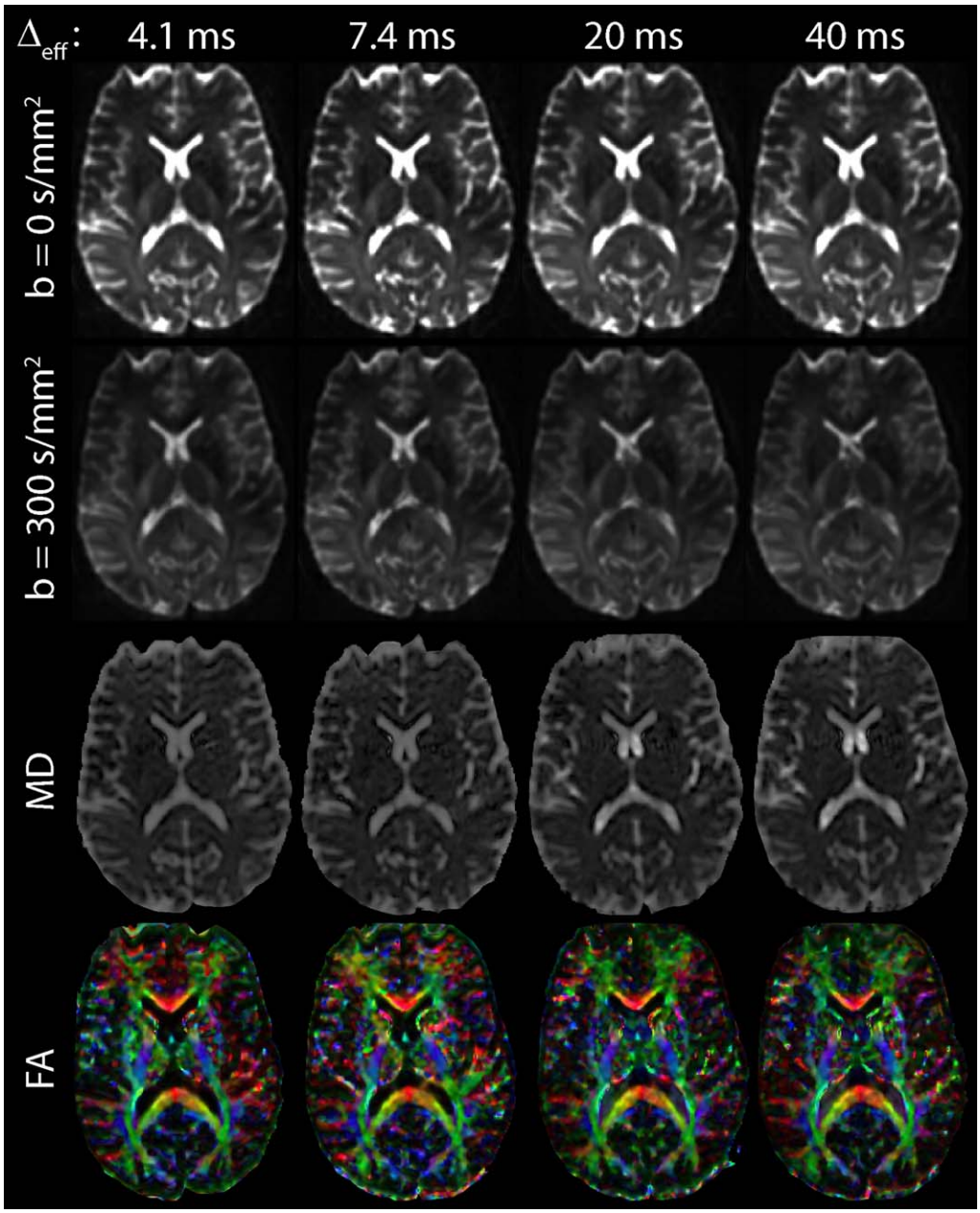

FIG. 4. Example raw data at b = 0 s/mm^2 and 300 s/mm^2 along with MD and FA (computed from the same data) color-coded with principal eigenvector direction for one subject. The images from the four diffusion times (4.1 ms OGSE, 7.4 ms OGSE, 20 ms PGSE, and 40 ms PGSE) are displayed using the same scale. [Color figure can be viewed in the online issue, which is available at wileyonlinelibrary.com.]

DTI and, thus, is more susceptible to errors from noise and residual Nyquist ghosting. To investigate this, the Δ_{eff} = 40 ms scan was performed at b-values of 300 and 1000 s/mm^2 in two subjects with all other imaging parameters identical (data not shown). Note that the Δ_{eff} = 40 ms, b300 scan had large durations where no gradients were played out in order for it to have the same TE as the OGSE scans (i.e., the TE was limited by the OGSE scans); therefore, it was possible to increase the diffusion gradient duration from 3.9 ms (Table 1) to 7.4 ms and change Δ_{eff} from 40 ms to 39 ms to attain b1000 without changing any other parameters in the pulse sequence. While the FA maps color coded with principal eigenvector direction had a similar qualitative appearance for the two scans, b300 generally resulted in smaller tracts and was more prone to false tracking than b1000. Nevertheless, tractography at b300 was capable of delineating the eight major white matter tracts that were investigated in this study. The two scans did not have noticeably different eddy current distortions (due to effective gradient precompensation—see above), and the extraction of DTI values within the tracts was evaluated by applying the tract masks obtained with b300 to both co-registered scans. Over all 10 regions, $\lambda_{||}$ changes ranged from 15% to 30% and $\lambda_{\perp}$ changes ranged from −19% to 29% for b300 relative to b1000. A −19% change in $\lambda_{\perp}$ in the genu was the only

negative change, and it arose due to a Gibbs ringing artifact that was most severely present in that tract. While the artifact varied with b-value, it was consistent with different Δ_{eff} at the same b-value. FA changes ranged from −4% to 10% in the eight white matter tracts. The consistent overall increase in ADC values is likely a result of the non-Gaussian nature of diffusion in brain tissue, where ADC values decrease for increasing b-values (33), while the small changes in FA are likely due to the greater sensitivity of the lower b-value data to noise; for example, in the CST the mean signal drop compared with b0 was 13% for b300 (mean SNR = 31) and 39% for b1000 (mean SNR = 21). Nevertheless, the results suggest that the smaller b-value did not have a large impact on the data quality within the regions studied, aside from a uniform shift in ADC values (perhaps with the exception of $\lambda_\perp$ in the genu).

RESULTS

The b = 0 s/mm^2 and b = 300 s/mm^2, as well as the diffusion parametric maps of mean diffusivity (MD, the average of the three eigenvalues) and FA, had similar qualitative appearance in the brain tissue over all four diffusion times (Fig. 4). Additionally, $\lambda_{||}$ and $\lambda_\perp$ appear qualitatively similar for Δ_{eff} = 4.1 ms compared with Δ_{eff} = 40 ms where difference images between the two diffusion times shows widespread increases in eigenvalues in brain tissue for the shorter diffusion time (Fig. 5). Even with a low b-value of 300 s/mm^2 the DTI images were of reasonable quality over much of the brain (Fig. 6), presumably due to the high SNR of greater than 50 (in the splenium) on b0 images for all the protocols.

In the water phantom, no significant variation of eigenvalues or FA was observed with respect to Δ_{eff}, and the very low FA of ~0.03 suggests high data quality (Fig. 7). In contrast, statistically significant variations of $\lambda_{||}$, $\lambda_\perp$, and FA were observed in the 7 healthy volunteers. For all white matter regions aside from $\lambda_{||}$ in the bCC, both eigenvalues increased significantly at the shorter OGSE diffusion times relative to the Δ_{eff} = 40 ms PGSE scan (Fig. 8). Very large proportional changes in ADC occurred in the SLF, with a 35% increase in $\lambda_\perp$ and 20% increase in $\lambda_{||}$ for Δ_{eff} = 4.1 ms relative to Δ_{eff} = 40 ms (Table 2). The other association tracts (CG, IFO, and ILF) had much smaller increases, near 10% for $\lambda_\perp$ and 15% for $\lambda_{||}$. In the sCC, gCC, and CST, ADC increases near 30% and 10% were observed for $\lambda_\perp$ and $\lambda_{||}$, respectively. Additionally, statistically significant decreases of FA to approximately −10% for diffusion times decreasing to 4.1 ms were observed in the bCC, sCC, CST, and SLF. Notably, FA reductions occurred because $\lambda_\perp$ increased by a larger proportion compared with $\lambda_{||}$ (Table 2). In the TH and PT, large increases in $\lambda_{||}$ and $\lambda_\perp$ of 16% and 18%, respectively (TH), and 16% and 26%, respectively (PT), were observed. The similar changes for $\lambda_{||}$ and $\lambda_\perp$ resulted in no clear trend in FA, and contrast the observations in half of the white matter tracts. While an FA increase was observed in the TH for Δ_{eff} = 7.4 ms, the variation in FA in that region was high and more prone to error due to its low value (34).

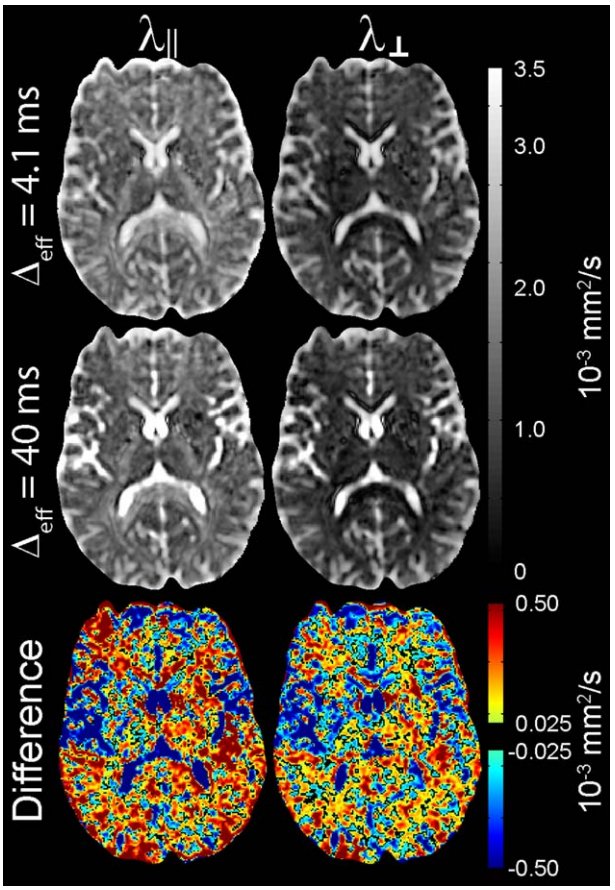

FIG. 5. Eigenvalue maps for the shortest (4.1 ms OGSE) and longest (40 ms PGSE) diffusion times (Δ_{eff}) and their difference (OGSE 4.1 ms − PGSE 40 ms). Widespread increases for both parallel and perpendicular eigenvalues are observed throughout the brain tissue as the diffusion time is reduced. Large ADC differences in the opposite direction are observed in CSF, particularly the lateral ventricles, due to elevated values (greater than free water at 37°C) in the 40 ms PGSE scan presumably due to flow artifacts. [Color figure can be viewed in the online issue, which is available at wileyonlinelibrary.com.]

DISCUSSION

This work demonstrates that OGSE DTI is feasible in the adult human brain and that a b-value of 300 s/mm^2 can yield adequate diffusion tensor parameterization for major white matter tracts and deep gray matter, provided that the SNR is sufficient. This is partially enabled by a trapezoidal gradient design, for which the equation for diffusion time has been introduced here. The key finding is that the diffusion tensor in human brain depends on diffusion time for Δ_{eff} as low as 4 or 7 ms in many white matter tracts and in deep gray matter. A diffusion time of 7 ms corresponds to a characteristic diffusion length of 4.6 μm, which defines a threshold of length scales where diffusion begins to become unrestricted (35). Given that typical axon dimensions in the human corpus callosum range from 0.5 to 3 μm, with a small number of axons as large as 10 μm (13,14), much larger changes in eigenvalues and FA may be observed for even smaller diffusion times because many more molecules would become unrestricted. That being said, cells other than

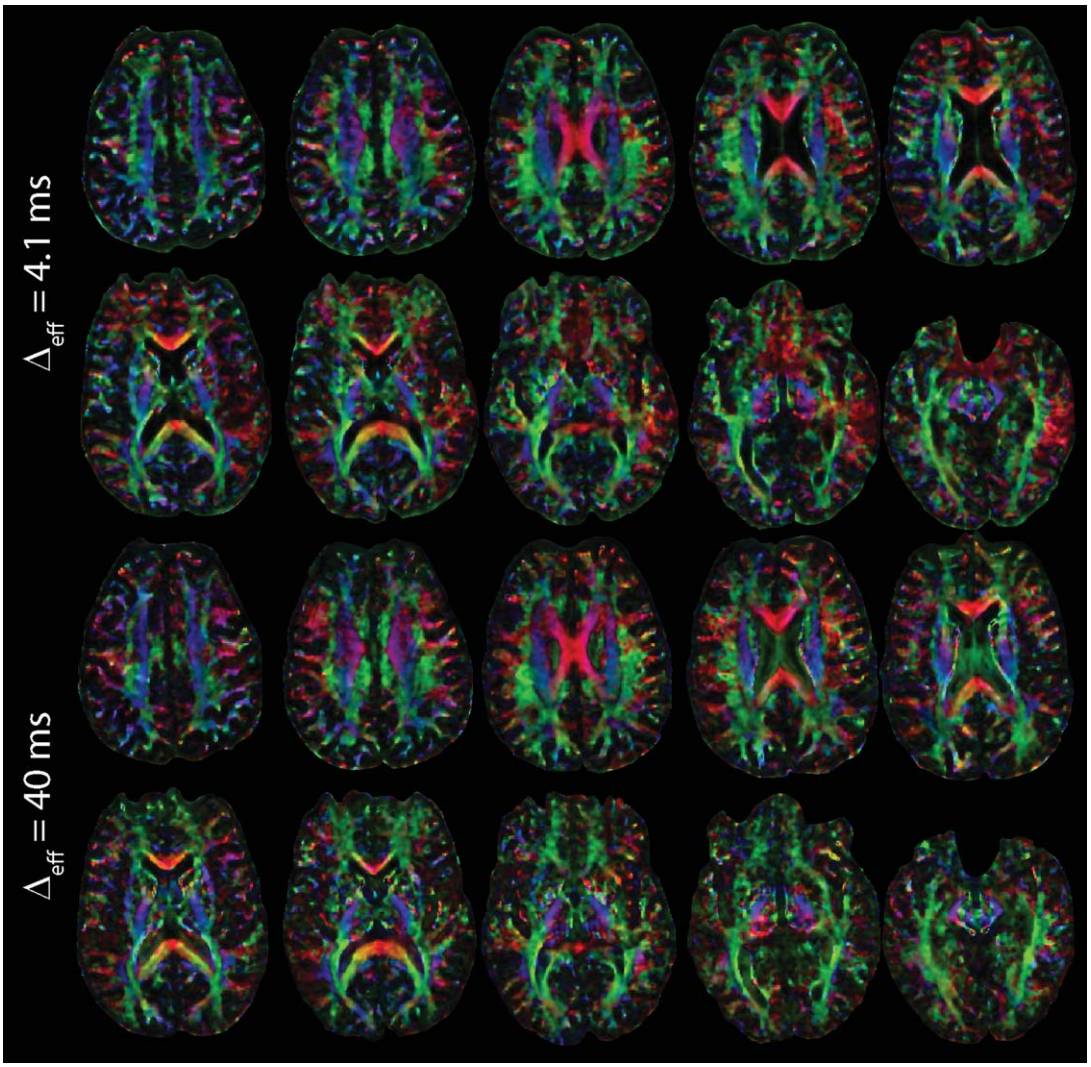

FIG. 6. Example data showing FA color-coded with principal eigenvector direction for one subject at diffusion times of 4.1 ms (OGSE) and 40 ms (PGSE). The images are very similar, particularly within the major white matter tracts that were of interest in this work.

axons likely contributed to the changes observed, such as the oligodendrocytes. These findings may explain the lack of Δ_{eff}-dependence observed previously (10–12), where the diffusion measurements used a larger minimum Δ_{eff} of 8 ms. Moreover, because the diffusion gradients contained spectral components at $f = 0$, in contrast to the cosine-like gradient waveforms used in this work, the previous PGSE experiments were not performed in a high-frequency regime (36). Notably, this work agrees with and expands upon the recent OGSE findings that suggested an increase of mean ADC in the splenium and genu of the human corpus callosum ranging from 5% to 50% for a diffusion time of 4 ms compared with 20 ms (27), compared with the increases of mean ADC found in the splenium (17%) and genu (18%) in this work (mean ADC, i.e., MD, not shown here, but readily calculated from the eigenvalues).

The overall finding in white matter that both $\lambda_{\perp}$ and $\lambda_{||}$ increase and FA decreases with substantially reduced Δ_{eff} agrees with some early findings in ex vivo nerve (6,7) and white matter of in vivo mouse (22). Using bipolar gradient pulses, one early study in excised frog sciatic nerve did not observe a change in $\lambda_{||}$ as diffusion time was reduced from 28 ms to 2 ms (5). Moreover,

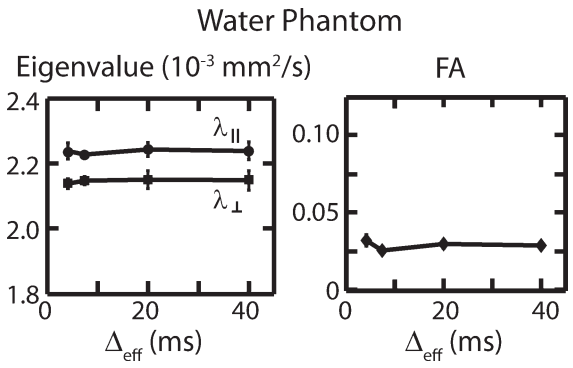

FIG. 7. Measurements of DTI eigenvalues and FA, which are very low at ~0.03, showing consistency in a $CuSO_4$ doped water phantom (N=4) at room temperature (22°C) as a function of diffusion time, Δ_{eff}.

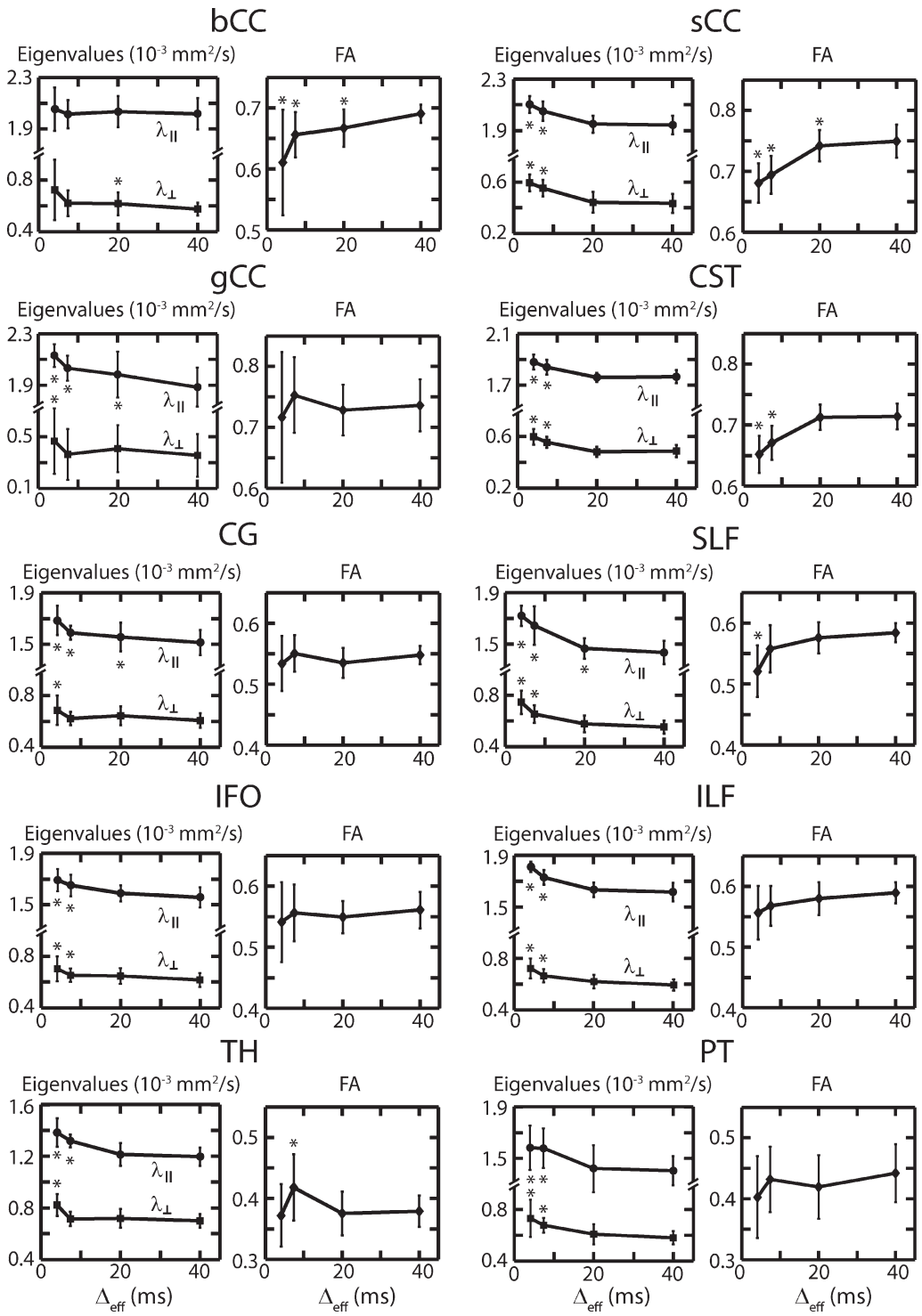

FIG. 8. Mean ± standard deviation of DTI eigenvalues and FA in 7 healthy human volunteers as a function of diffusion time, Δ_{eff}, for Δ_{eff} values of 4.1 ms (OGSE), 7.4 ms (OGSE), 20 ms (PGSE), and 40 ms (PGSE). Statistical significant deviations from the $\Delta_{eff} = 40$ ms scan determined using a paired t-test are denoted with *($P < 0.05$). Increasing parallel ($\lambda_{||}$) and perpendicular ($\lambda_{\perp}$) eigenvalues for reduced Δ_{eff} are observed in all white matter regions except the bCC, while decreasing FA for reduced Δ_{eff} is observed only in the bCC, sCC, CST, and SLF. In the deep gray matter (TH and PT), both eigenvalues increase with decreasing Δ_{eff}; however, there is no clear trend of FA. Region abbreviations are as in Figure 3.

over the same OGSE frequency range as here (0 to 50 Hz), $\lambda_{\perp}$ and $\lambda_{||}$ increases of approximately 30% and 10%, respectively, and FA decreases of 5% were observed in mouse white matter in vivo (22), which is comparable to our findings. The Δ_{eff} for which ADC values approach an asymptotic value defines a transition to a regime where the free water diffusion distance is several times larger than the surrounding tissue microstructure. Therefore,

Table 2
Mean Percent Change (± SD) of $\lambda_{||}$, $\lambda_{\perp}$, and FA for Diffusion Times of 4 ms (OGSE) Relative to 40 ms (PGSE) in Seven Healthy Subjects [a]

	$\lambda_{||}$ (%)	$\lambda_{\perp}$ (%)	FA (%)
bCC	2 ± 3	24 ± 29	−12 ± 12*
sCC	8 ± 4*	40 ± 22*	−9 ± 4*
gCC	14 ± 10*	32 ± 21*	−3 ± 10
CST	6 ± 3*	23 ± 9*	−9 ± 4*
CG	11 ± 2*	13 ± 11*	−3 ± 7
SLF	20 ± 4*	35 ± 14*	−11 ± 8*
IFO	9 ± 6*	14 ± 13*	−4 ± 8
ILF	12 ± 5*	22 ± 16*	−6 ± 6
TH	16 ± 6*	18 ± 10*	−2 ± 12
PT	16 ± 8*	26 ± 26*	−8 ± 18

[a]Values with statistical significance using a paired t-test ($P < 0.05$) are denoted by asterisks.

because the FA decreased for short Δ_{eff} in the bCC, sCC, CST, and SLF, it is probable that more molecules transitioned from a restricted to unrestricted regime in the perpendicular direction compared with the parallel direction as the diffusion time was decreased, likely because the perpendicular direction had more molecules in a restricted regime to begin with. This rationale coincides with the observations of larger eigenvalue changes in the perpendicular direction compared with the parallel direction. This is appropriate given the highly anisotropic microstructural dimensions of white matter. The FA only decreased for smaller Δ_{eff} in half of the white matter tracts, as it did not significantly change in the ILF, IFO, gCC, and CG, because the proportional increases in $\lambda_{||}$ and $\lambda_{\perp}$ were similar. This finding suggests that the anisotropy in these tracts stems from smaller length scales than those accessed by the minimum diffusion time of 4 ms. This may suggest smaller axon diameters compared with the other tracts. This finding agrees with histological findings in the corpus callosum, where the axons in the genu are smaller than in the body and splenium (13). The finding of similar increases of both $\lambda_{\perp}$ and $\lambda_{||}$ with decreasing Δ_{eff} in the thalamus and putamen agrees with observations of deep gray matter in rodents (21,22). Thus, there were no changes of FA, which is consistent with "isotropic" length scales of microstructure (averaged over each voxel) expected in gray matter. Also, the increases in mean ADC of approximately 10–15% that were observed in the rodent deep gray matter for OGSE frequencies from 0 to 50 Hz are comparable to our findings.

Geometric dispersion of axons (i.e., fanning), particularly in the association tracts, may have contributed to differences in the eigenvalues and FA with Δ_{eff}. The degree of axon dispersion varies for different white matter tracts (37), but is less plausible to have affected the results for the central portions of the genu and splenium of the corpus callosum. The axon dispersion effectively creates some mixing of perpendicular and parallel diffusion. Note that crossing fibers would result in a similar effect. This may also explain why changes in parallel eigenvalues were observed here for most tracts, but not previously in an excised frog sciatic nerve which has highly ordered axons and presumably little dispersion (5). However, excised nerves have other underlying microstructural differences (e.g., edema) relative to in vivo. Another alternative explanation is that changes in parallel eigenvalues at short diffusion times may be due to restriction effects of water in isotropic cells, such as oligodendrocytes, in the white matter. Another potential consideration in the interpretation of these results are the effects of different diffusion gradient pulse durations for the different scans (Table 1), where longer gradient pulses can lead to an apparent narrowing of restricted geometry and reduction of the signal drop expected from diffusion (38). This effect has been shown to decrease with b-value, and for b-values of 1000 s/mm^2 it was negligible in a rat sciatic nerve with gradient durations ranging from 2 to 32 ms (39). As such, at the very low b-value of 300 s/mm^2, it is unlikely that this phenomenon affected the results.

It was evident in the processed diffusion maps that the MD and FA for water in the cerebrospinal fluid (CSF) became elevated beyond expected values and less uniform for the PGSE scans with longer Δ_{eff} (Figs. 4–6). The origin of this is likely turbulent flow of CSF, which would have long effective "diffusion" distances and, thus, only the long Δ_{eff} PGSE scans with gradient frequency components (i.e., F(f) in Eq. [2]) equal to zero are sensitive to it. Moreover, the OGSE waveform used is inherently velocity-compensated (27), which reduces first order flow effects. Nonuniform MD and FA in CSF is not observed in typical PGSE DTI acquisitions because the much larger b-values (1000 s/mm^2 instead of 300 s/mm^2) are not as sensitive to flow. Averaging over all the ventricular space in all subjects, this flow-sensitivity led to higher $\lambda_{\perp}$ of 5% (OGSE (2.9 ± 0.09) × 10^{-3} mm^2/s, PGSE (3.0 ± 0.2) × 10^{-3} mm^2/s), $\lambda_{||}$ of 19% (OGSE (3.22 ± 0.02) × 10^{-3} mm^2/s, PGSE (3.8 ± 0.4) × 10^{-3} mm^2/s), and FA of 115% (OGSE 0.07 ± 0.02, PGSE 0.15 ± 0.03) for PGSE (Δ_{eff} = 40 ms) relative to the OGSE (Δ_{eff} = 4 ms) in CSF, which is in the opposite direction to the diffusion parameter changes seen in brain tissue. The above values also demonstrate that the flow effects were highly subject dependent. Notably, diffusion time dependence of ADC in CSF with very large intersubject variation has been mentioned for in vivo rat brain measured with low b-value of 400 s/mm^2 (21).

The primary limitation of the OGSE methodology for human in vivo applications is the long TE of 110 ms required to yield a minimally acceptable b-value of 300 s/mm^2 given our single axis gradient strength of 60 mT/m. At this long TE, particularly at 4.7T, the SNR in some regions with or near high concentrations of iron was not sufficient for analysis, such as in the basal ganglia (note: this problem will be worse at 7T and higher). The long TE also resulted in very high CSF signal, which exacerbated Gibbs ringing and partial volume effects adjacent to the ventricles and cortex; as such this precluded tractography in small tracts near CSF, such as the fornix, and measurements in the cortex (also limited by spatial resolution).

The ability to accurately identify the onset of Δ_{eff}-dependence may provide insight into microstructure changes that occur in pathology. With recent advances in hardware enabling gradients as large as 100 or 200mT/m on custom-built human MRI scanners, higher

b-values and/or OGSE frequencies (i.e., lower diffusion times) will be achievable with OGSE. For example, a frequency as high as 100 Hz at a b-value of 1000 s/mm^2 could be possible with 200 mT/m gradients; however, slew rate constraints would have to be carefully considered. Given that the minimum diffusion time of 4 ms in this work is likely only small enough to circumvent restricted diffusion in larger axons, much larger changes in DTI parameters will likely occur with shorter minimum diffusion times (and higher frequencies), as shown in the animal models. Furthermore, a larger range of Δ_{eff} may enable quantitative measurements such as nuclear size or surface to volume ratios in the in vivo human brain, which may give new understanding into the mechanisms underlying tissue changes observed in disease, such as the still not well understood ADC decreases observed in ischemic stroke.

CONCLUSIONS

In conclusion, this work has demonstrated the feasibility of acquiring OGSE DTI in the human brain, and that DTI eigenvalues and FA depend on the diffusion time over 4 to 40 ms in both white matter tracts and deep gray matter. The ability to target different length scales by means of the diffusion time may improve sensitivity to changes in tissue microstructure associated with particular pathologies.

ACKNOWLEDGMENTS

The authors thank the Canadian Institutes of Health Research for operating funds, as well as Alberta Innovates – Health Solutions (CB, CAB) and the Natural Sciences and Engineering Research Council (CAB) for salary support. MRI infrastructure was provided by the Canada Foundation for Innovation, Alberta Science and Research Authority, Alberta Heritage Foundation for Medical Research, and the University Hospital Foundation.

REFERENCES

1. Beaulieu C, Allen PS. Water diffusion in the giant axon of the squid: implications for diffusion-weighted MRI of the nervous system. Magn Reson Med 1994;32:579–583.
2. Takahashi M, Hackney DB, Zhang G, Wehrli SL, Wright AC, O'Brien WT, Uematsu H, Wehrli FW, Selzer ME. Magnetic resonance microimaging of intraaxonal water diffusion in live excised lamprey spinal cord. Proc Natl Acad Sci U S A 2002;99:16192–16196.
3. Tanner JE, Stejskal EO. Restricted self-diffusion of protons in colloidal systems by the pulsed-gradient, spin-echo method. J Chem Phys 1968;49:1768–1777.
4. Stejskal EO, Tanner JE. Spin diffusion measurements: spin echoes in the presence of a time-dependent field gradient. J Chem Phys 1965; 42:288–292.
5. Beaulieu C, Allen PS. An in vitro evaluation of the effects of local magnetic-susceptibility-induced gradients on anisotropic water diffusion in nerve. Magn Reson Med 1996;36:39–44.
6. Seo Y, Morita Y, Kusaka Y, Steward MC, Murakami M. Diffusion of water in rat sciatic nerve measured by H-1 pulsed field gradient NMR: compartmentation and anisotropy. Jpn J Physiol 1996;46:163–169.
7. Stanisz GJ, Henkelman RM. Diffusional anisotropy of T2 components in bovine optic nerve. Magn Reson Med 1998;40:405–410.
8. Bar-Shir A, Cohen Y. High b-value q-space diffusion MRS of nerves: structural information and comparison with histological evidence. NMR Biomed 2008;21:165–174.
9. Niendorf T, Norris DG, Leibfritz D. Detection of apparent restricted diffusion in healthy rat brain at short diffusion times. Magn Reson Med 1994;32:672–677.
10. Lebihan D, Turner R, Douek P. Is water diffusion restricted in human brain white-matter - an echo-planar NMR imaging study. Neuroreport 1993;4:887–890.
11. Clark CA, Hedehus M, Moseley ME. Diffusion time dependence of the apparent diffusion tensor in healthy human brain and white matter disease. Magn Reson Med 2001;45:1126–1129.
12. Nilsson M, Latt J, Nordh E, Wirestam R, Stahlberg F, Brockstedt S. On the effects of a varied diffusion time in vivo: is the diffusion in white matter restricted? Magn Reson Imaging 2009;27:176–187.
13. Aboitiz F, Scheibel AB, Fisher RS, Zaidel E. Fiber composition of the human corpus callosum. Brain Res 1992;598:143–153.
14. Alexander DC, Hubbard PL, Hall MG, Moore EA, Ptito M, Parker GJM, Dyrby TB. Orientationally invariant indices of axon diameter and density from diffusion MRI. Neuroimage 2010;52:1374–1389.
15. Gross B, Kosfeld R. Application of spin-echo method in measurement of auto-diffusion. Messtechnik 1969;77:171.
16. Schachter M, Does MD, Anderson AW, Gore JC. Measurements of restricted diffusion using an oscillating gradient spin-echo sequence. J Magn Reson 2000;147:232–237.
17. Gore JC, Xu J, Colvin DC, Yankeelov TE, Parsons EC, Does MD. Characterization of tissue structure at varying length scales using temporal diffusion spectroscopy. NMR Biomed 2010;23:745–756.
18. Xu J, Does MD, Gore JC. Dependence of temporal diffusion spectra on microstructural properties of biological tissues. Magn Reson Imaging 2011;29:380–390.
19. Xu J, Does MD, Gore JC. Quantitative characterization of tissue microstructure with temporal diffusion spectroscopy. J Magn Reson 2009; 200:189–197.
20. Novikov DS, Kiselev VG. Surface-to-volume ratio with oscillating gradients. J Magn Reson 2011;210:141–145.
21. Does MD, Parsons EC, Gore JC. Oscillating gradient measurements of water diffusion in normal and globally ischemic rat brain. Magn Reson Med 2003;49:206–215.
22. Aggarwal M, Jones MV, Calabresi PA, Mori S, Zhang J. Probing mouse brain microstructure using oscillating gradient diffusion MRI. Magn Reson Med 2012;67:98–109.
23. Kershaw J, Leuze C, Aoki I, Obata T, Kanno I, Ito H, Yamaguchi Y, Handa H. Systematic changes to the apparent diffusion tensor of in vivo rat brain measured with an oscillating-gradient spin-echo sequence. Neuroimage 2013;70:10–20.
24. Harkins KD, Galons J-P, Divijak JL, Trouard TP. Changes in intracellular water diffusion and energetic metabolism in response to ischemia in perfused C6 rat glioma cells. Magn Reson Med 2011;66:859–867.
25. Xu J, Does MD, Gore JC. Sensitivity of MR diffusion measurements to variations in intracellular structure: effects of nuclear size. Magn Reson Med 2009;61:828–833.
26. Xu J, Li K, Smith RA, Waterton JC, Zhao P, Chen H, Does MD, Manning HC, Gore JC. Characterizing tumor response to chemotherapy at various length scales using temporal diffusion spectroscopy. PLoS ONE 2012;7:e41714.
27. Van AT, Holdsworth SJ, Bammer R. In vivo investigation of restricted diffusion in the human brain with optimized oscillating diffusion gradient encoding. Magn Reson Med 2014;71:83–94.
28. Parsons EC, Does MD, Gore JC. Modified oscillating gradient pulses for direct sampling of the diffusion spectrum suitable for imaging sequences. Magn Reson Imaging 2003;21:279–285.
29. Ianuş A, Siow B, Drobnjak I, Zhang H, Alexander DC. Gaussian phase distribution approximations for oscillating gradient spin echo diffusion MRI. J Magn Reson 2013;227:25–34.
30. Portnoy S, Flint JJ, Blackband SJ, Stanisz GJ. Oscillating and pulsed gradient diffusion magnetic resonance microscopy over an extended b-value range: implications for the characterization of tissue microstructure. Magn Reson Med 2013;69:1131–1145.
31. Jensen DJ, Brey WW, Delayre JL, Narayana PA. Reduction of pulsed gradient settling time in the superconducting magnet of a magnetic resonance instrument. Med Phys 1987;14:859–862.
32. Jehenson P, Westphal M, Schuff N. Analytical method for the compensation of eddy-current effects induced by pulsed magnetic field gradients in NMR systems. J Magn Reson (1969) 1990;90:264–278.

33. Mulkern RV, Gudbjartsson H, Westin C-F, et al. Multi-component apparent diffusion coefficients in human brain. NMR Biomed 1999; 12:51–62.
34. Farrell JAD, Landman BA, Jones CK, Smith SA, Prince JL, van Zijl PCM, Mori S. Effects of signal-to-noise ratio on the accuracy and reproducibility of diffusion tensor imaging–derived fractional anisotropy, mean diffusivity, and principal eigenvector measurements at 1.5T. J Magn Reson Imaging 2007;26:756–767.
35. Sukstanskii AL, Ackerman JJH, Yablonskiy DA. Effects of barrier-induced nuclear spin magnetization inhomogeneities on diffusion-attenuated MR signal. Magn Reson Med 2003;50:735–742.
36. Sukstanskii AL. Exact analytical results for ADC with oscillating diffusion sensitizing gradients. J Magn Reson 2013;234:135–140.
37. Zhang H, Schneider T, Wheeler-Kingshott CA, Alexander DC. NODDI: practical in vivo neurite orientation dispersion and density imaging of the human brain. Neuroimage 2012;61:1000–1016.
38. Mitra PP, Halperin BI. Effects of finite gradient-pulse widths in pulsed-field-gradient diffusion measurements. J Magn Reson Ser A 1995;113:94–101.
39. Yeh C-H, Tournier JD, Cho K-H, Lin C-P, Calamante F, Connelly A. The effect of finite diffusion gradient pulse duration on fibre orientation estimation in diffusion MRI. Neuroimage 2010;51:743–751.